

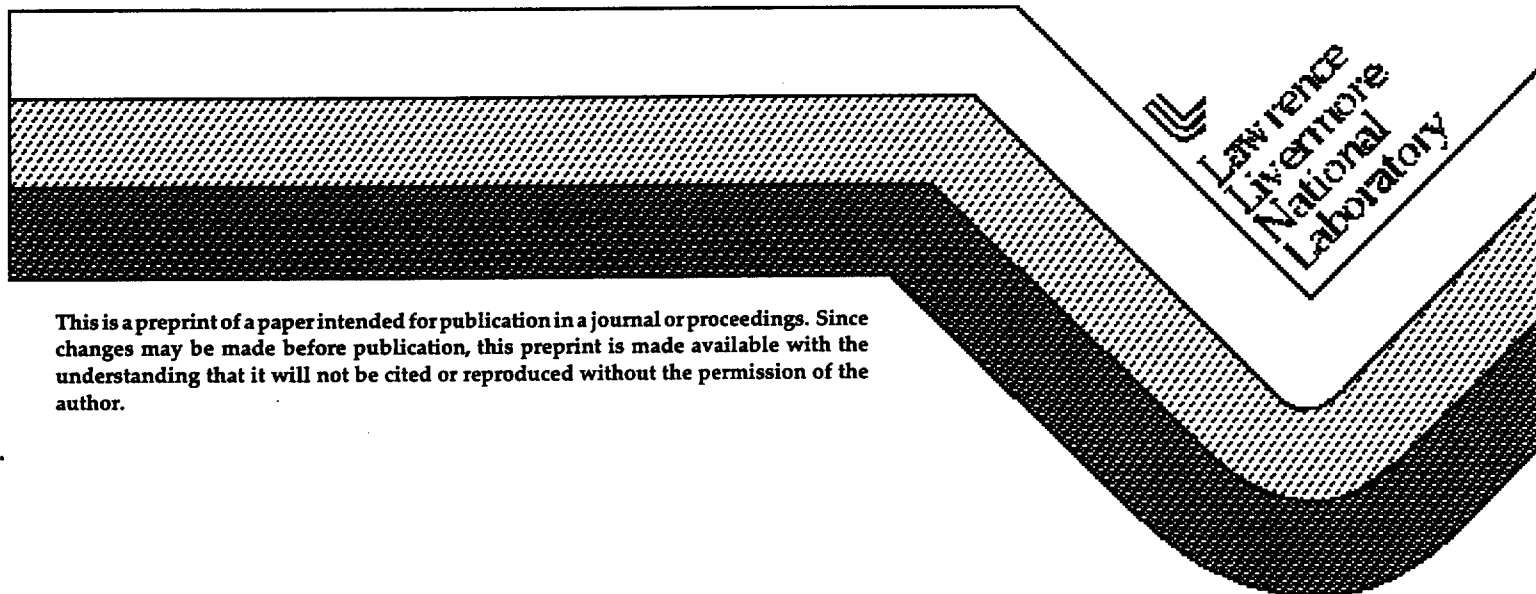
# Microstructure and Kinetics of Hot Corrosion for a Nickel Alloy in Molten Salt

D. W. Stevens and W. A. Brummond  
Lawrence Livermore National Laboratory

D. L. Grimmett, J. C. Newcomb, K. T. Chiang, R. L. Gay  
Energy Technology Engineering Center, Rocketdyne Division  
Boeing North American, Inc.

This paper was prepared for presentation to the  
29th Annual International Metallographic Society Convention  
Pittsburgh, PA, July 21-24, 1996

December 1996



This is a preprint of a paper intended for publication in a journal or proceedings. Since changes may be made before publication, this preprint is made available with the understanding that it will not be cited or reproduced without the permission of the author.

#### DISCLAIMER

This document was prepared as an account of work sponsored by an agency of the United States Government. Neither the United States Government nor the University of California nor any of their employees, makes any warranty, express or implied, or assumes any legal liability or responsibility for the accuracy, completeness, or usefulness of any information, apparatus, product, or process disclosed, or represents that its use would not infringe privately owned rights. Reference herein to any specific commercial product, process, or service by trade name, trademark, manufacturer, or otherwise, does not necessarily constitute or imply its endorsement, recommendation, or favoring by the United States Government or the University of California. The views and opinions of authors expressed herein do not necessarily state or reflect those of the United States Government or the University of California, and shall not be used for advertising or product endorsement purposes.

# MICROSTRUCTURE AND KINETICS OF HOT CORROSION FOR A NICKEL ALLOY IN MOLTEN SALT

D. W. Stevens and W. A. Brummond

Lawrence Livermore National Laboratory  
University of California  
Livermore, CA 94550

D. L. Grimmer, J. C. Newcomb, K. T. Chiang, R. L. Gay

Energy Technology Engineering Center, Rocketdyne Div., Boeing North American, Inc.  
Canoga Park, CA

## Abstract

Metallography, analytical scanning electron microscopy, and X-ray diffraction were employed to measure the kinetics and characterize the microstructure of hot corrosion of a Ni-Cr-Fe alloy, INCONEL 600\*, after 500h of immersion in molten  $\text{Na}_2\text{CO}_3$ -NaCl salt at 900-950°C in an oxidizing atmosphere. This was done to help assess the alloy as a reaction-vessel material for a waste treatment process known as Molten Salt Oxidation.

The alloy was found to hot corrode by surface oxidation and intergranular attack, IGA. Their combined rate for the loss of load-bearing cross-section metal was comparable to corrosion rates reported by others for an array of analogous salts. About 5% of the oxide scale was a contiguous, dense, protective layer of  $\text{Cr}_2\text{O}_3$  at the metal/oxide interface. A middle portion comprised about 55% of the scale and was a porous, mixed oxide of  $\text{NiO} > \text{Cr}_2\text{O}_3 > \text{Fe}_2\text{O}_3$ . The outer 40% was nearly all  $\text{NiO}$  with dense grains and cavitated grain boundaries. Overall, the  $\text{NiO}$  was dominant and the lesser amounts of  $\text{Cr}_2\text{O}_3$  and  $\text{Fe}_2\text{O}_3$  were roughly equivalent. No direct invasion of salt through the oxide to the metal was observed.

## Introduction

Molten Salt Oxidation (MSO) is a waste destruction process currently under development to treat wastes that could be treated by incineration. In MSO, the organic portion of the waste is destroyed by catalytic reaction in a liquid carbonate-base salt bath at about 900-950°C. The bath is lanced with 20% excess air to maintain a highly oxidizing environment. This converts the C and H components of the organic wastes (oil, solvents,

plastic, cloth, rubber, paper, etc.) to  $\text{CO}_2$  and  $\text{H}_2\text{O}$ , respectively. Inorganic residues, including radioactive materials, are trapped in the molten salt and ultimately removed and processed into a final, nonleachable ceramic. The reaction vessel for this process must be made of metal in order to transfer heat from the exothermic chemical reactions and the process is corrosive to metal.

Considerable literature exists on the corrosion of materials in molten salts<sup>1,2</sup>. Corrosion studies and reviews in molten carbonate melts have been reported as part of studies on heat transfer and energy storage media,<sup>3-6</sup> coal gasification,<sup>7,8</sup> and molten carbonate fuel cells<sup>9</sup>. In general, the corrosion rate has been shown to depend on salt composition with carbonate melts generally being less corrosive than hydroxide melts.<sup>10,11</sup> Temperature and the oxidizing level of the gas environment are also important factors affecting the corrosion rate. Small amounts of certain elements in the salt, such as sulfur or chlorine, may increase the corrosion rate. INCONEL 600 and Incoloy 800 were cited as preferred alloys for use in molten carbonates by Kohl et al.<sup>5</sup> In unpublished work, the present authors selected INCONEL 600 over Incoloy 800 and other likely alloys by corrosion-test screening. An Arrhenius plot by Kohl et al of INCONEL 600 corrosion rates in various molten alkali metal carbonate salts was replotted and is given in Fig. 1, which also contains a preview of the results obtained in this work.

The salts employed by others in Fig. 1 included Na, K, and Li (alone or combined), chloride, and hydroxide. The cover gases varied considerably and included argon, air, air- $\text{CO}_2$  mixtures, and  $\text{CO}_2$ . Unfortunately, none of the test conditions (temperature, salt, and gas) were sufficiently close to those employed in MSO to be of significant value. Also, the wide scatter of the data raised strong doubts about interpreting it. The next step—and the purpose of this work—was to determine the effect of temperature on hot corrosion of INCONEL 600 under MSO conditions and to characterize the resulting microstructures.

\*Nominal composition: 74Ni (+Co)-16Cr-8Fe-2 other (wt%). UNS designation is NO6600. INCONEL is a trademark of the Inco family of companies.

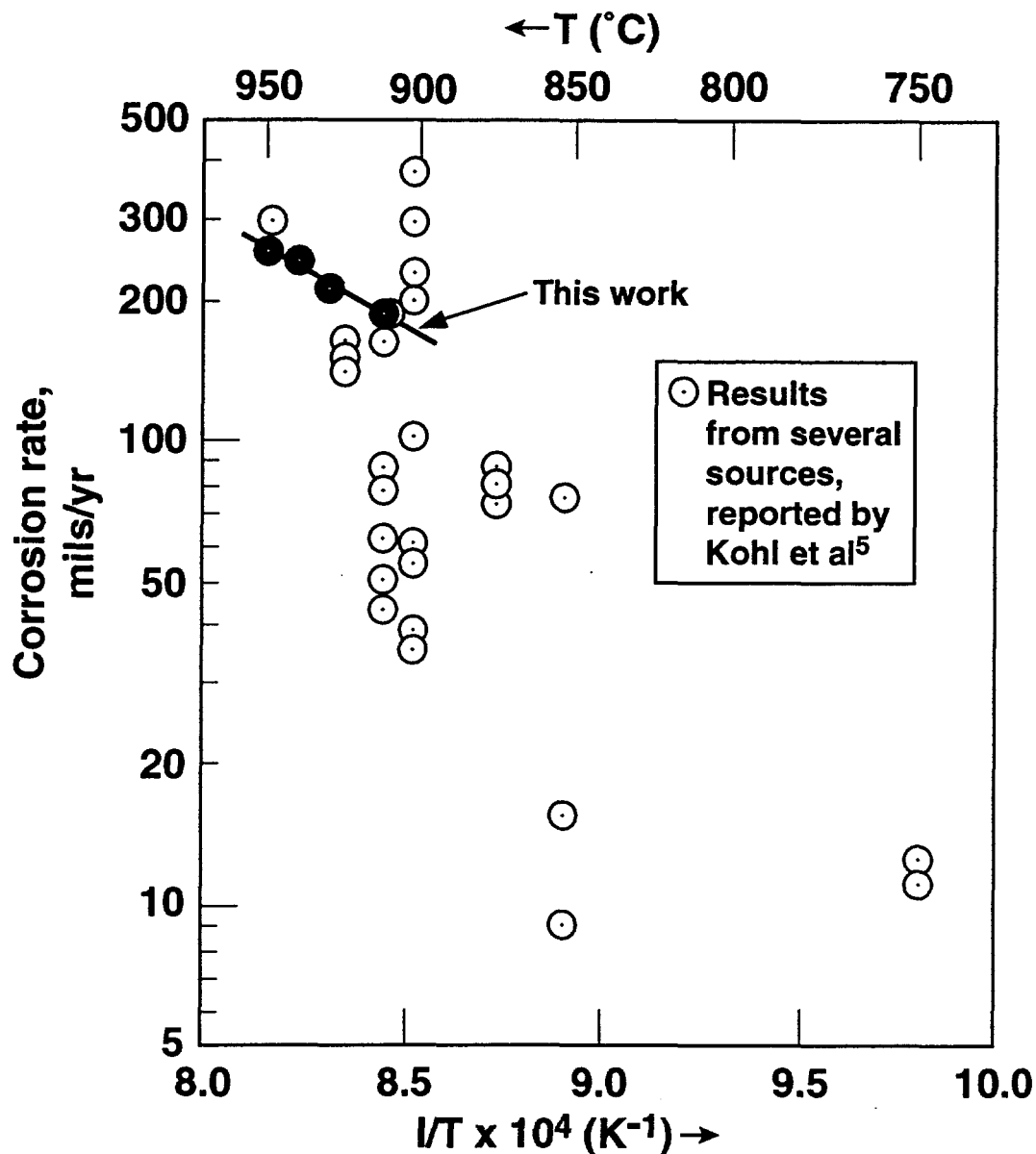


Fig. 1 – Rate of hot corrosion of INCONEL 600 in molten alkali metal carbonate salts.

#### Experimental Procedure

INCONEL 600 was corrosion tested for 500h at five temperatures between 900 and 950°C (900, 908, 929, 941, and 950°C) under prototypical MSO conditions in the salt furnace system shown in Fig 2. The sample resting on the bottom of the 2.5"-ID alumina tube represents a 6" X 1" X 1/8" bar of mill-annealed plate with a bright, 120-grit finish. Thickness was measured before testing to the nearest 0.0001" along every 1/4" of the bar length. A hole near the top of the bar allowed wire hooking for loading and unloading. The

molten salt was Na<sub>2</sub>CO<sub>3</sub> – 20 mol% NaCl, blended from reagent-grade NaCl and ACS-grade Na<sub>2</sub>CO<sub>3</sub>. The sparge gas of 8.6% CO<sub>2</sub>, 10.2%O<sub>2</sub> and 81.2%N<sub>2</sub> exited a Matheson Type 602 rotameter at 200cc/min. and became saturated by bubbling through water held at 109°F by an oil bath tank (Blue M "Magni Whirl"). The gas at this point represented the MSO process and is referred to further here as "MSO-type gas". The gas proceeded along tape-heated lines to the furnace where it bubbled through the melt, then exited the system through glycerin in a bubble jar at 1–2 bubbles/s. Type K thermocouples were

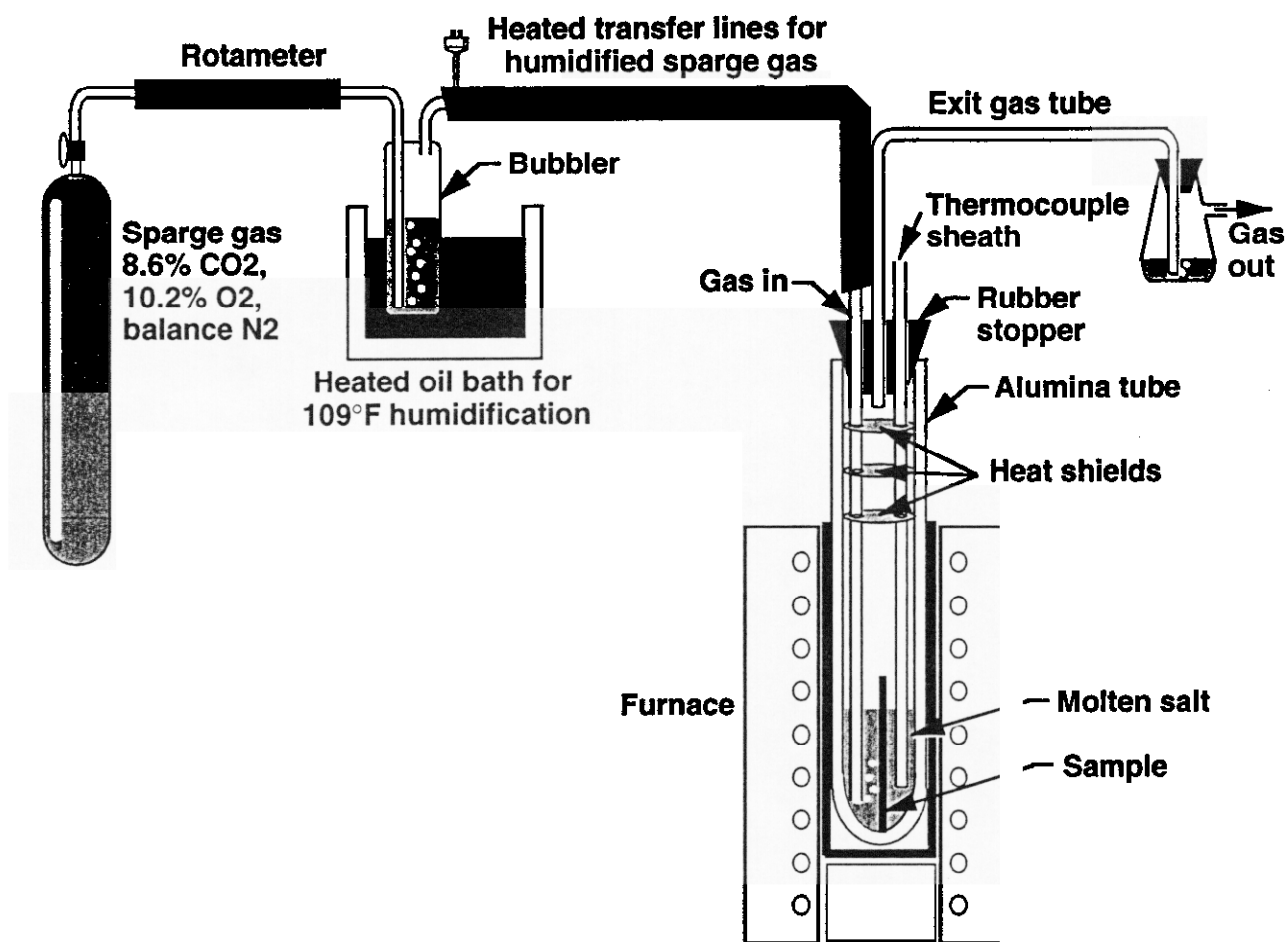


Fig. 2 – Schematic view of the salt furnace system.

employed in the computerized furnace controller and thermal data was accessed through a separate computer.

After testing, salt was ultrasonically washed from the bars in hot water. The bars were slit along their lengths and examined microscopically to determine the relative extent of attack along their lengths. It was found that corrosion was rather uniform along the salt-submerged portion of the bar but was slightly greater, or as deep as anywhere else, about 1" below the salt line. This portion was therefore cut from all five bars, then metallographically prepared and examined with a light optic metallograph (LOM).

It was found that the microstructures of the surface oxides and metal were analogous for all five samples and that the kinetics varied predictably with temperature. Therefore, one of the samples was selected to represent all five for additional

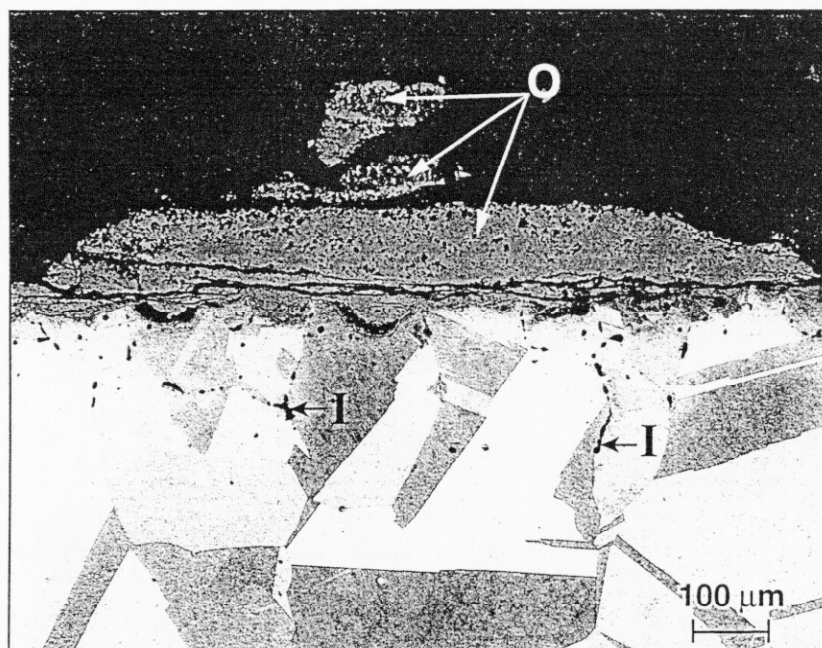
analysis by X-ray diffraction (XRD) and analytical SEM analysis. The 900°C sample was selected because more of its surface oxide had survived spalling. The XRD was done on a Phillips XPERT diffractometer with Cu K<sub>α</sub> at 40KV. The sample was loaded intact with its oxide facing the beam. This yielded patterns from the entire oxide thickness and part of the underlying metal. JCPDS files were employed for phase identification. The analytical SEM analysis was done with a JEOL model JSM 840 Scanning Electron Microscope 840 with a Tracor Northern model TN-5500 energy dispersive X-ray (EDX) analyzer.

All micrographs were processed electro-optically by scanning at 300 lines/in., adjusting with Adobe Photoshop®, and printing at 600 dpi.

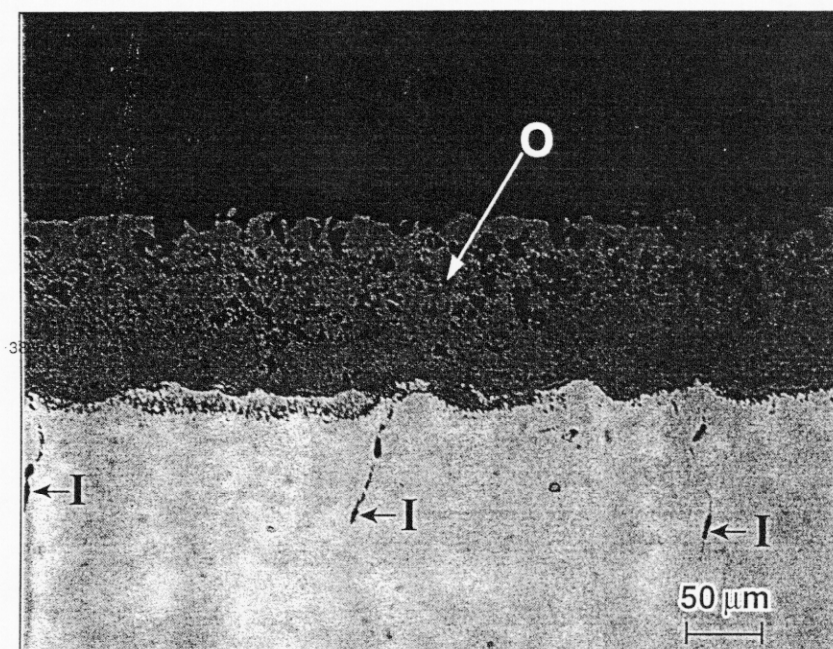
## Results and Discussion

The modes of hot corrosion attack observed here between 900° and 950°C were oxidation and IGA, as shown in Fig. 3. All five samples exhibited

analogous microstructures, the only notable differences being the thickness and spalling of the oxide, and the depth of IGA. The microstructural features in Fig. 3 required to measure the extent of corrosion attack are depicted schematically in Fig. 4.



**a) 950°C                      etched                      LOM**



**b) 900°C                      as-polished                      SEM**

**Fig. 3 – Oxidation (O) and IGA (I) of INCONEL 600 after 500 h at 900° or 950°C in  $\text{Na}_2\text{CO}_3$  – 20 mol% NaCl salt with MSO-type gas.**

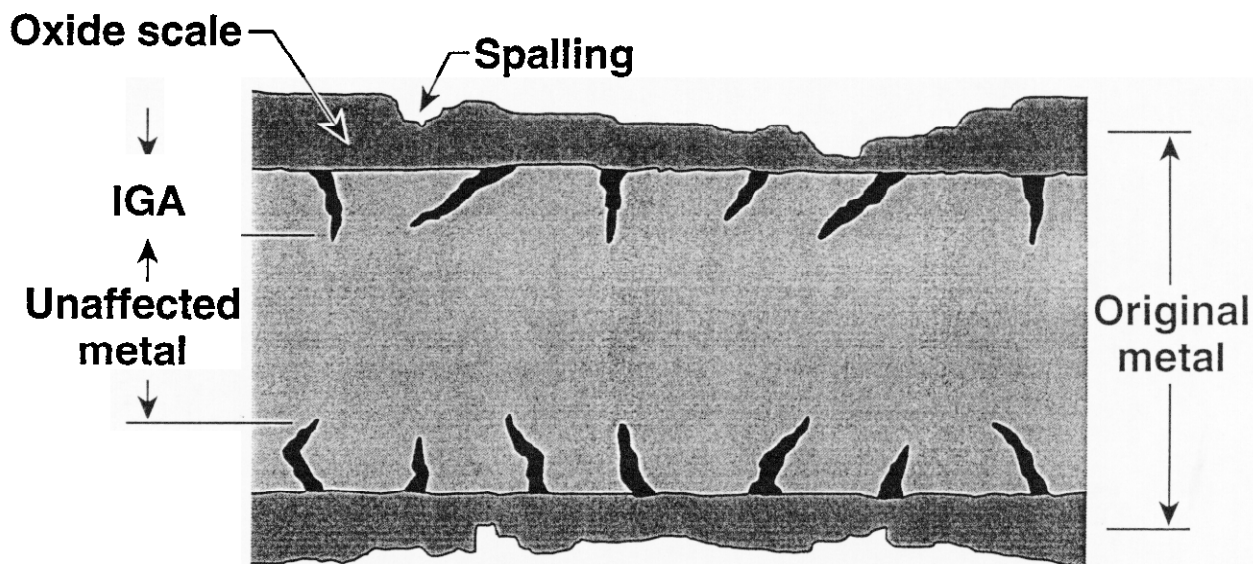


Fig. 4 – Metallography to measure metal loss from corrosion.

It can be seen from Fig. 4 that the loss of load-supporting cross-section metal from hot corrosion is the sum of the metal thickness consumed by oxidation plus the depth of the IGA penetration.<sup>\*</sup> The extent of IGA is defined here as the amount remaining in the survived metal and not the total amount that occurred from the outset. It is measured directly from the deepest penetrations to account for the worst case. The loss from oxidation is the original metal thickness minus the remaining metal bounded by the oxide/metal interface, divided by 2 to account for only one surface being corroded. This method is described in the standard, ASTM G54-77.<sup>12</sup> Making these measurements on the samples (the 900°C sample was omitted because its starting thickness was not certain), and converting them from 500 h to 1 yr to obtain mils/yr, yielded the hot corrosion rates in Fig. 5.

<sup>\*</sup>It was observed here that gravimetry and electrochemistry measurements were sometimes extended erroneously in studies such as this. To understand this, note that only the unaffected metal depicted in Fig. 4 is capable of fully supporting design loads. This critical dimension is revealed by metallography but not by gravimetry or electrochemistry measurements, even though results from these latter two methods are often interpreted erroneously as total measures of corrosion. For examples, gravimetry is completely confounded by oxidation weight gain and spalling, and internal attack cannot be quantified by either gravimetry or electrochemical measurements. Certainly, these two methods do serve invaluable roles in characterizing certain aspects of hot corrosion, but these roles do not apply here.

The oxidation plot in Fig. 5 follows Arrhenius behavior whereas IGA appears to be independent of temperature. Their total (shown earlier in Fig. 1) displays Arrhenius behavior. As seen from Fig. 1, the hot corrosion rates obtained here are consistent with and encompassed by those obtained from a wide variety of roughly comparable corrosion variables.

XRD of the oxide of the 900°C sample revealed the presence of three oxides, NiO, Cr<sub>2</sub>O<sub>3</sub>, and Fe<sub>2</sub>O<sub>3</sub>. The distribution of these oxides is revealed in Figs. 6 – 8, which contain SEM images in the SE (secondary electron) and BSE (back-scattered electron) modes, as well as EDX elemental maps and EDX point analyses. SE imaging is employed to yield detail and resolution, whereas BSE images distinguish heavier elements from lighter ones (the heavier, the brighter). Ni is heavier than Cr and Fe is in between. In Fig. 6, the common area of the SEM images is seen in the lower row as reduced-magnification elemental maps obtained by EDX. Note the intense Cr at the metal/oxide interface and the corresponding lack of Ni and Fe. This corresponds to the Cr<sub>2</sub>O<sub>3</sub> layer indicated in Fig. 7b) and is confirmed by point E analysis seen in Fig. 8a) and d). Thus, the Cr<sub>2</sub>O<sub>3</sub> layer on the metal is seen to be contiguous and dense, indicative of a protective layer. It occupies about 5% of the total oxide thickness.

Local chemical analysis of points D and C in Fig. 8 show a transition away from the Cr<sub>2</sub>O<sub>3</sub> layer into increasing amounts of NiO and Fe<sub>2</sub>O<sub>3</sub>, mostly

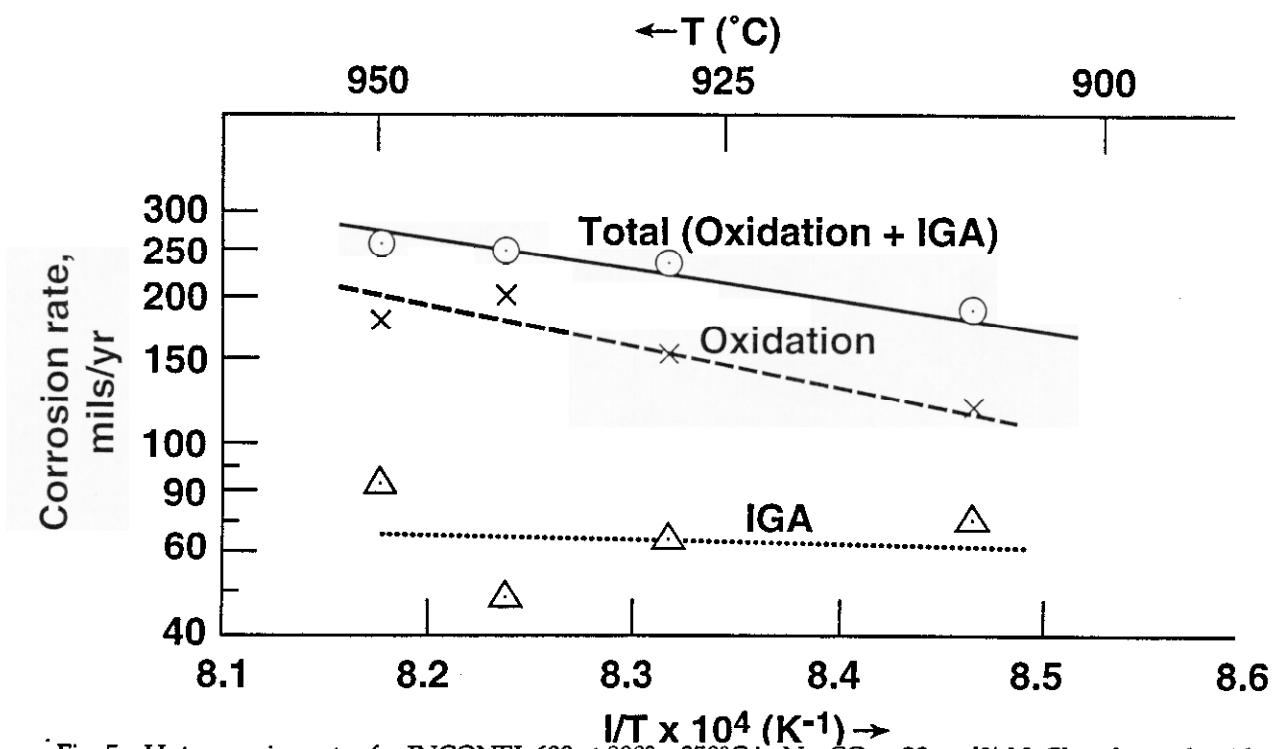


Fig. 5 – Hot corrosion rates for INCONEL 600 at 900° – 950°C in  $\text{Na}_2\text{CO}_3$  – 20 mol% NaCl molten salt with MSO-type gas.

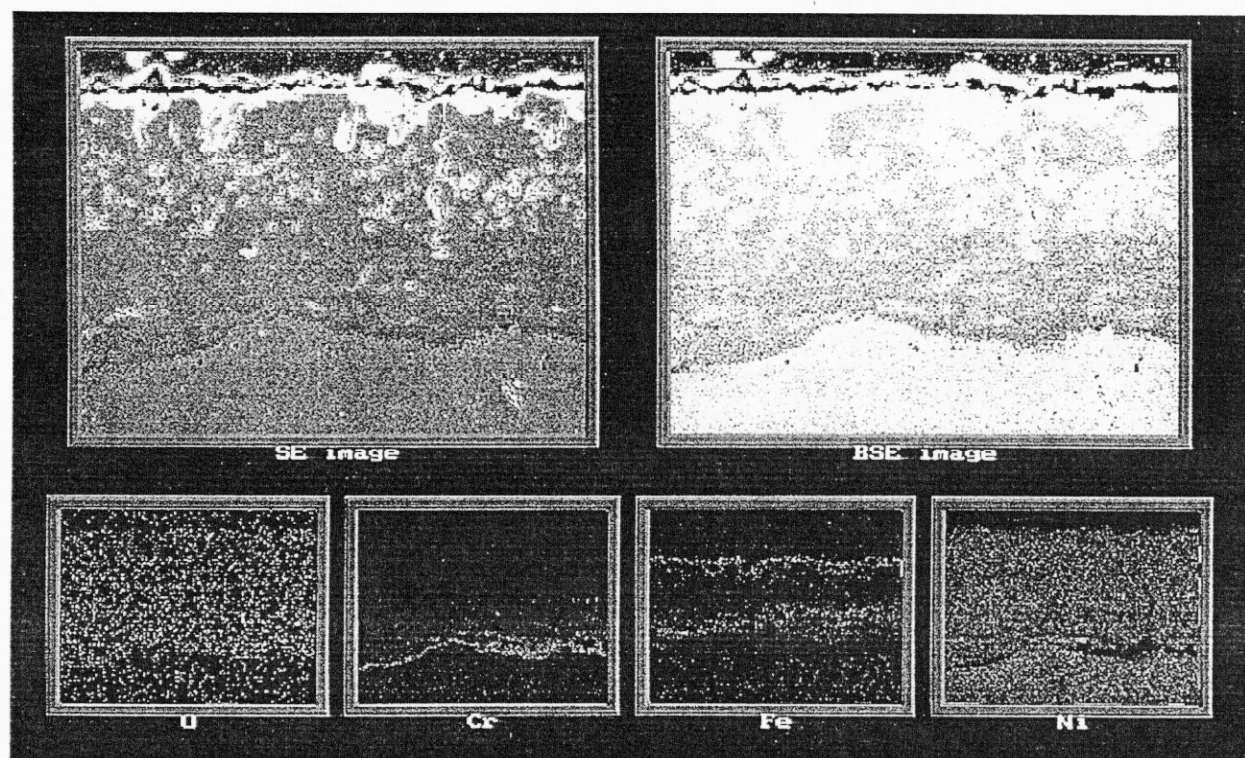


Fig. 6 – SEM/EDX analysis of the metal and oxide of INCONEL 600 after 900°C/500 h in molten salt.

NiO. This three-oxide, middle region where  $\text{NiO} > \text{Cr}_2\text{O}_3 > \text{Fe}_2\text{O}_3$  comprises about 55% of the oxide and is seen in Fig. 7a) to be moderately porous. Note in this broad band that the  $\text{Fe}_2\text{O}_3$  was somewhat segregated in the two bands seen in Fig. 6, where the lower band is seen in detail at point C in Figs. 8a) and b).

The EDX spectra of points A and B in Fig. 7a) are given in c) and d). They indicate that the top portion of the oxide scale is mostly NiO with a very small amount of  $\text{Fe}_2\text{O}_3$ . It is seen in Fig. 7a) that the grains of this mostly-NiO scale are very dense and have cavitated grain boundaries. This outer portion accounts for about 40% of the oxide scale.

Considering the entire oxide scale, NiO was the dominant phase, and the smaller quantities of the  $\text{Cr}_2\text{O}_3$  and  $\text{Fe}_2\text{O}_3$  phases were roughly equivalent.

No evidence of internal salt was observed by metallography, XRD, or analytical SEM, indicating that salt did not invade the metal through the oxide.

### Conclusions

INCONEL 600 subjected to molten salt corrosion between 900° and 950°C exhibited surface oxidation and intergranular attack (IGA). Their combined Arrhenius rates are consistent with those obtained by others under roughly comparable conditions.

The oxide scale exhibited three regions. Covering the metal was a contiguous, dense, protective layer of  $\text{Cr}_2\text{O}_3$ . The midsection was a porous mix of  $\text{NiO} > \text{Cr}_2\text{O}_3 > \text{Fe}_2\text{O}_3$ . The top portion was nearly all NiO with dense grains and cavitated grain boundaries.

No direct invasion of salt through the oxide to the metal was observed.

### Acknowledgments

Most of the metallographic preparation and preliminary analysis was skillfully performed by Robert Kershaw.

### References

<sup>1</sup>G. J. Janz and R.P.T. Tomkins, *Corrosion*, **35**, No. 11, p. 485 (1979).

<sup>2</sup>G. Y. Lai, "High Temperature Corrosion of Engineering Alloys," Chapter 9 in *"Molten Salt Corrosion,"* ASM International, Materials Park, OH (1990).

<sup>3</sup>R.T. Coyle, R. W. Burrows, R. M. Goggin, T. M. Thomas, "Exploratory Corrosion Tests on Materials and Fluids for Advanced High-Temperature Molten-Salt Storage," Solar Energy Research Institute/TR-255-2199, Oct. 1984.

<sup>4</sup>R. T. Coyle, T. M. Thomas, Schissel, "The Corrosion of Selected Alloys in Eutectic Lithium-Sodium-Potassium, Carbonate at 900°C," Solar Energy Research Institute/PR-255-2561, Jan. 1986.

<sup>5</sup>A. L. Kohl, J. C. Newcomb, W. R. Castle, "Evaluation of a Conical Tank for High Temperature Molten Salt Containment," Rockwell International/RD86-295, Canoga Park, CA, Jan. 1987.

<sup>6</sup>R. J. Petri, T.D. Claar, E. T. Ong, "High Temperature Molten Salt Thermal Energy Storage Systems for Solar Applications," DOE/NASA/0156-83/1, NASA CR-167916, July 1983.

<sup>7</sup>C. A. Kuster, "Metals and Metal Alloys for Coal Gasification Process Molten Salt, Survey of Corrosion Testing," Atomics International, San Diego, CA, #N423MAR420-001, Feb. 1976.

<sup>8</sup>Rockwell International, Canoga Park, CA, "Black Liquor Gasification Phase 2B Final Report, Part 4, Materials Evaluation," Atomics International-DOE-13546.

<sup>9</sup>M-L. Saboungi, H. Kojima, ed., *Proceedings of the Int. Symp. on Molten Salt Chemistry and Technology*, 93-9, p. 321, 436, The Electrochemical Society, Inc., (1993).

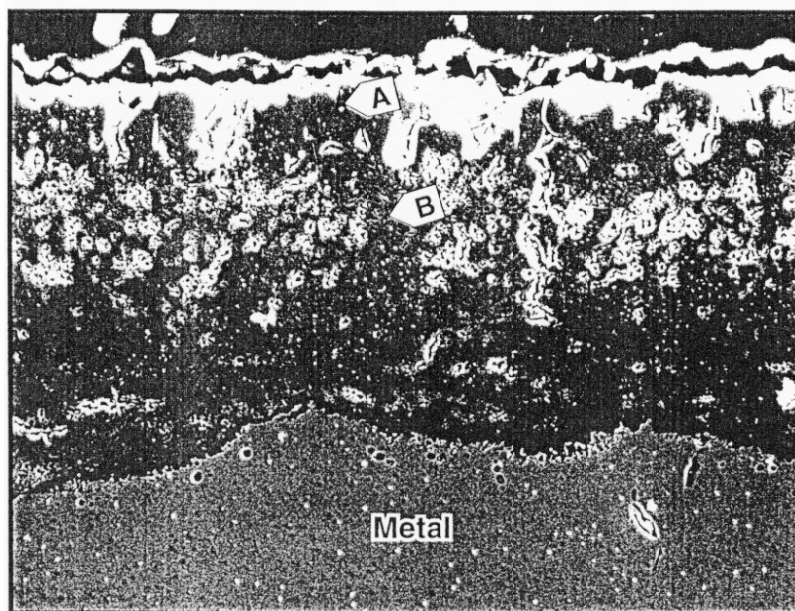
<sup>10</sup>G. Y. Lai, reference 2, p. 180

<sup>11</sup>J. H. Jackson and M. H. LaChance, as cited in G. Y. Lai, p. 170.

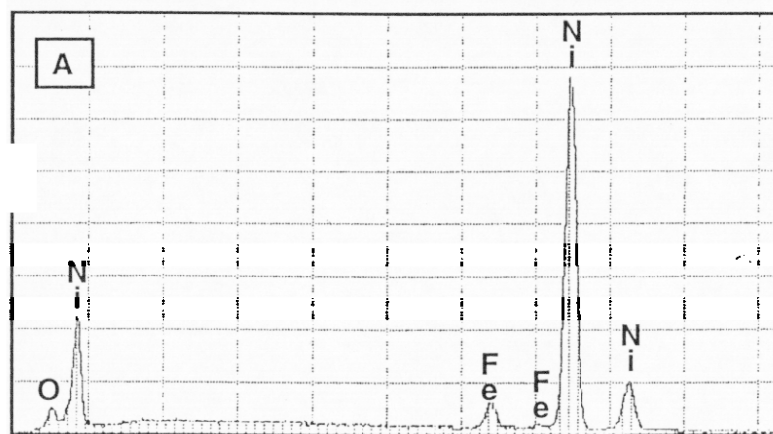
<sup>12</sup>American Society for Testing of Materials, Philadelphia, PA

This work was performed under the auspices of the U.S. Department of Energy by the Lawrence Livermore National Laboratory under contract number W-7405-ENG-48.

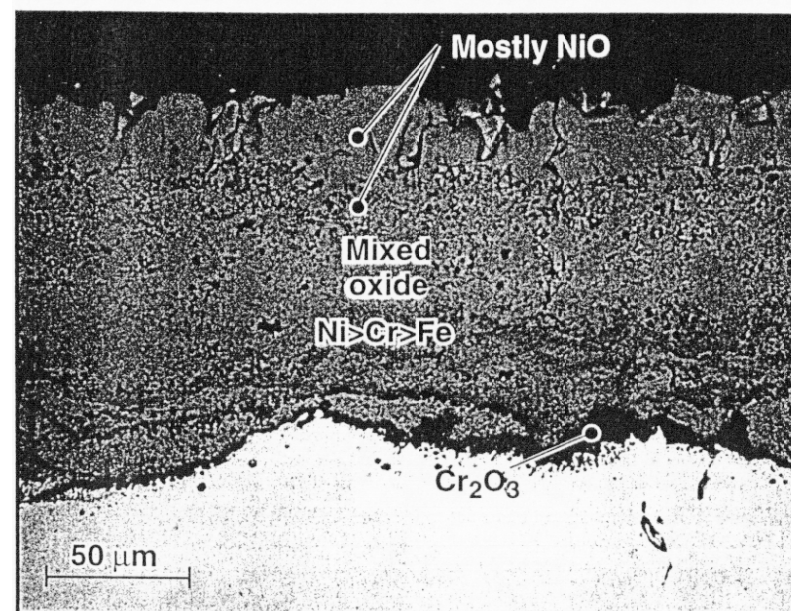
Fig. 7 - SEM/EDX analysis of the top region of the oxide scale on INCONEL 600 after 900°C/500 h in molten salt.



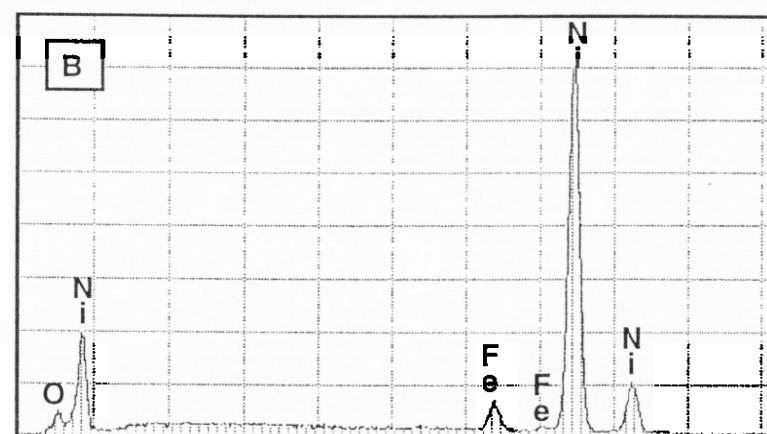
a) SE image



c) EDX of point A

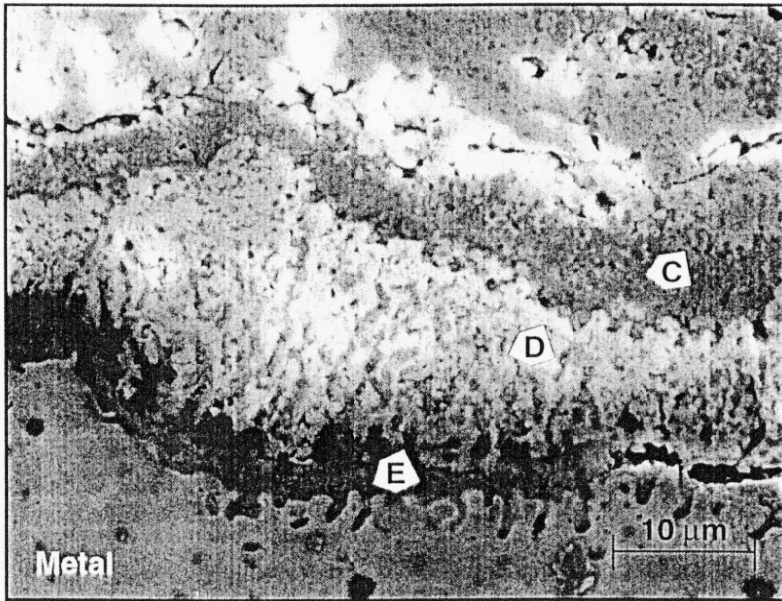


b) BSE image

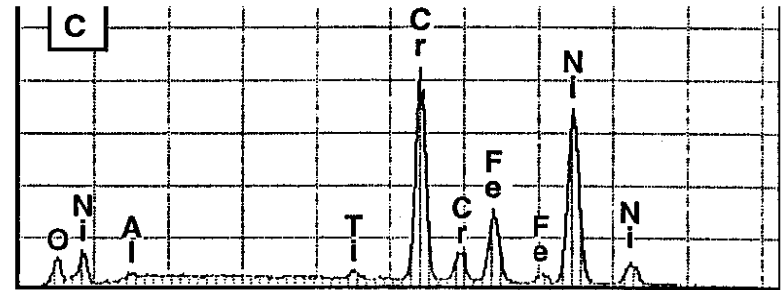


d) EDX of point B

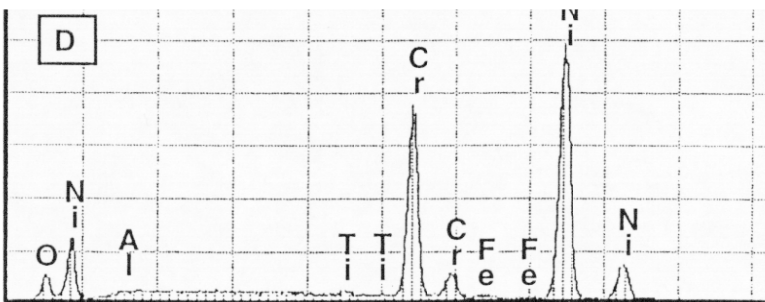
Fig. 8 ~ SEM/EDX analysis of the oxide/metal interface of Inconel 600 after 900°C/500 h in molten salt.



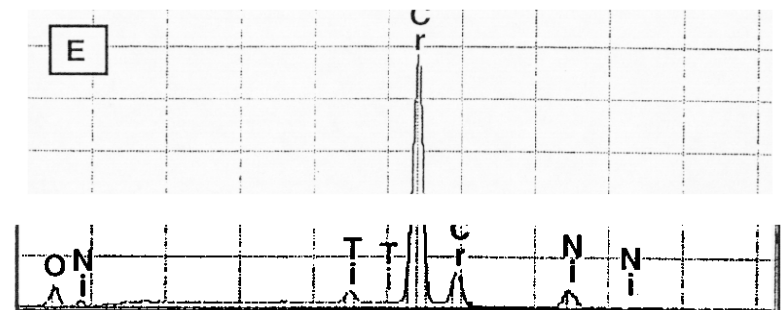
a) SEM of oxide-metal region (corrosion front)



b) EDX of point C



c) EDX of point D



d) EDX of point E